**Climate Dynamics 2008** DOI:10.1007/s00382-008-0389-3

# The three dimensional structure of the atmospheric energy budget: methodology and evaluation

Kevin E. Trenberth and Lesley Smith

National Center for Atmospheric Research[1]
P. O. Box 3000
Boulder, CO 80307

email: trenbert@ucar.edu
ph: (303) 497 1318
fax: (303) 497 1333

11 December 2007
Revised 11 February 2008

## *Abstract*

Studies of the vertically-integrated energy and moisture budgets of the atmosphere are expanded to three dimensions. The vertical integrals of the moisture, energy and heat budget equations computed analytically act as a very strong constraint on any local computational results of the vertical structure. This paper focuses on the methodology and difficulties in closing the budgets and satisfying constraints, given the need to use a pressure coordinate because model coordinates all differ. Vertical interpolation destroys delicate mass balances and can lead to inconsistencies, such as from how geopotential or vertical motion is computed. Using the advective rather than flux form of the equations greatly reduces the contamination from these effects. Results are documented for January 1989 using European Centre for Medium Range Weather Forecasts (ECMWF) reanalysis (ERA-40) data.

The moistening, diabatic heating and total energy forcing of the atmosphere are computed as a residual from the analyses using the moisture, dry energy (dry static energy plus kinetic energy) and total atmospheric (moist static plus kinetic) energy equations. The components from the monthly averaged flow and transients, as a function of layer in the atmosphere, and as quasi-horizontal and vertical fluxes of dry static, latent and kinetic energy are examined. Results show the moistening of the atmosphere at the surface, its release as latent heat in precipitation and transformation into dry static energy, and thus net radiative cooling as a function of height and location. The vertically integrated forcings computed from the model parameterizations are compared with available observations and budget-derived values, and large ERA-40 model biases are revealed in radiation and precipitation. The energy and moisture budget-derived quantities are more realistic, although results depend on the quality of the analyses which are not constructed to conserve mass, moisture or energy, owing to analysis increments.

Keywords: Atmospheric energy, atmospheric moisture, atmospheric vertical structure, reanalyses, model biases.

[1] The National Center for Atmospheric Research is sponsored by the National Science Foundation.

## 1. Introduction

A focus of our work over recent years has been documenting the flow of energy through the climate system (Trenberth et al. 2002a; Trenberth and Stepaniak 2003a,b; 2004), its variability (Trenberth et al. 2002b,c) and especially the role of water (Trenberth et al. 2005, 2007). The main focus has been on the bulk vertically-integrated atmospheric energy and moisture budgets. Using various datasets, we have estimated the incoming shortwave solar radiation, its total conversion into other energy forms (internal energy, sensible heat, latent energy, potential energy, dry static energy, moist static energy, kinetic energy), the storage and changes in storage (tendency) of these components, the transport by atmospheric winds and ocean currents, the surface fluxes and exchanges between the atmosphere and ocean, and the further transformation into radiant longwave energy as it is radiated back to space (Trenberth and Stepaniak 2004). Several recent studies have deduced the ocean heat storage and transports as a residual of the energy budget (Fasullo and Trenberth 2008a,b; Trenberth and Fasullo 2008) based on estimates of the surface heat fluxes (Trenberth et al. 2001), and compared results with ocean data to obtain a more holistic view of the energy flows and their uncertainties. Errors can be estimated by making use of multiple estimates of the same quantity using different data and methods, and the closure of the budgets.

In the current study, we expand the analysis of the atmospheric energetics and heat budget to examine the full three dimensional spatial structure. This paper focuses on the methodology and difficulties in closing the budgets, and therefore documents the results for only one month, January 1989, in detail as a follow on to Trenberth et al. (2002a), who used the same month to document computational issues for the vertically-integrated energy quantities. The energy and heat budget equations can be vertically integrated analytically and the results computed directly. Thus because the vertical integral is known, it acts as a very strong constraint on any local computational results of the vertical structure. Therefore we have used this as a test and constraint on methods.

The most accurate computations are possible in the model coordinates of the numerical weather prediction model used for data assimilation. One common vertical coordinate has been a "sigma" terrain-following coordinate, where the surface pressure is the first level, and all other levels are normalized by the surface pressure, throughout the atmosphere, such as has been used by the National Centers for Environmental Prediction/National Center for Atmospheric Research (NCEP/NCAR) reanalyses (referred to as NRA). More generally, hybrid coordinates are similar at the bottom of the atmosphere but transition to pressure levels in the stratosphere, somewhere near 100 hPa. The sigma and hybrid coordinates vary from day to day with the surface pressure and are distorted over topography in ways that have been shown to cause erroneous pathological features in the NRA reanalyses (Trenberth and Stepaniak 2002). The framework varies from one institution to another because even if the coordinate system is the same, the choice of levels generally varies. Moreover, we wish to be able to compare results with climate model output that, in turn, is on yet a different vertical coordinate. For these reasons, it is highly desirable to adopt a standardized vertical pressure coordinate framework for diagnostics. But the disadvantage is that accuracy is lost as variables are interpolated vertically from the hybrid to pressure coordinates. Also the available archives of pressure level analyses have quite coarse vertical resolution, and we strongly recommend that they be revised to be 25 hPa below 700 hPa and 50 hPa resolution or better in the rest of the troposphere.

Several respects of these computations are extremely demanding and are not straightforward. A prerequisite for determining the energy budget and energy transports is to have a balanced closed mass budget. Otherwise, there is an implied return flow, mandated by continuity, somewhere else that is transporting energy. This means that fluxes of energy in part of the atmosphere, such as the upper troposphere, should not be interpreted as transports because they do not take account of the return flow, such as in the lower troposphere in the Hadley Circulation. Yet this is not an uncommon approach (e.g., Tian et al. 2001). Hence, for budget computation of any quantity, it is essential to also examine and balance the dry air mass budget (Trenberth 1991a; 1997) and substantial adjustments are required to the energy terms to obtain sensible results. Interpolations almost inevitably ruin any such balance and it either has to be restored, for instance by re-computing the vertical motion from the horizontal components, mass weighted, or other adjustments made. The more natural form of the equations to use in tracking flows of energy are the so-called flux forms, but these prove to be much more sensitive to small computational errors, and thus the advective forms of the equations prove to have most utility. We describe and illustrate these aspects in sections 2 and 3.

Very often energy budgets have been formulated with approximate equations that either leave out the kinetic energy equation (e.g., Yu et al. 1999) or more commonly formulate a dry static energy equation (e.g., Yanai et al. 1973; 1976) when no such equation is valid. It is almost equivalent to dropping the kinetic energy component and has been perpetuated in many further studies, such as Tian et al. (2001) (and see references therein), while other studies ignore the heating from

frictional dissipation (e.g., Johnson and Cielieski 2000). Trenberth et al. (2002a) showed that these approximations are not acceptable for quantitative results, although frictional heating is very small.

The NRA have been used to deduce the diabatic heating by Yanai and Tomita (1998), but they used the pressure level archive with only twice daily values, so that the semidiurnal tide is aliased in their results. Hoskins and Sardeshmuhk (1987) used the thermodynamic equation in potential temperature form for their diagnosed heat budget without mass constraints. Yu et al. (1999) used both NCEP and ECMWF reanalyses to compute zonal mean divergences of atmospheric energy transports and also use pressure level analyses, but without the constraints imposed here. Tendency terms have been widely ignored on the grounds that averaging in time reduces them to become negligible. However, this is not the case for monthly or seasonal time scales (Trenberth et al. 2002a) and they are small enough to ignore only with averages over many years.

In addition, strong dynamical constraints on the flow mandate relationships among various energy components. If internal energy is increased through an increase in temperature, then the atmospheric column expands and thus alters the potential energy. Prior to condensation, atmospheric flow tends to be isentropic, and rising air cools at the dry adiabatic lapse rate, further ensuring a strong link between sensible heat and potential energy. The latter are combined in the concept of dry static energy. A parcel of air near sea level has high sensible heat and small potential energy, but when lifted to the upper troposphere, sensible heat is lost through adiabatic cooling while the potential energy increases. Also, low level mass divergence has to be compensated by upper level mass convergence, or vice versa, so that divergence of energy fluxes has enormous compensation in the vertical by design. Similar concepts apply to moist static energy when condensation takes place, except that a rising air parcel cools at the saturated adiabatic lapse rate, and it is the departures from the saturated adiabatic lapse rate in the vertical and their co-variability with velocity that determine net meridional energy transports. Other diabatic processes generally act on slower time scales and are of less consequence.

Section 2 discusses the data used and the physical background and mathematical expressions for the energy and moisture budgets and their breakdown into components. Section 3 presents results for the month of January 1989.

## 2. Three dimensional moisture and energy budgets.

In this paper, the data used are from the European Centre for Medium Range Weather Forecasts (ECMWF) reanalyses, known as ERA-40 (Uppala et al. 2005). The full resolution four-times daily data on model coordinates have been used to obtain the best accuracy possible for the vertical integrals. ERA-40 analyses have a horizontal resolution of T-159 and 60 levels in the vertical. Replication of the full vertical integrals is a necessary condition before we can have confidence in a break down of the vertically integrated transports into contributions by layers. An evaluation of temperature fields from ERA-40 by Trenberth and Smith (2006) showed how the vertical structure of the temperature field varied from 1979 to 2001 using ERA-40 data and found some fundamental problems in the vertical structure associated with problems in biases arising from the changing observing system (especially instruments on satellites), and errors from how Mount Pinatubo aerosols had interfered with radiances. Therefore, there are questions about the validity of ERA-40 results overall. Here we confine our attention to January 1989 as the fields are much better than those in the 1990s (Uppala et al. 2005) and we will not address time series here. The use of 6-hourly analyses captures the diurnal cycle reasonably well but still leaves out higher frequency information which can lead to errors of order 10% in individual terms even in a full model framework (Boville 1985).

These computations are done in such a way that the vertical integral sums to the result of the vertical mean budgets computed separately. A central focus is on understanding the processes involved in temperature changes at different levels in the atmosphere and the link to the changes to diabatic heating. Processes involved in maintaining static stability and temperature lapse rate are characterized by contributions to the heat budget by transient eddies and mean flow broken down into quasi-horizontal and vertical fluxes of dry static, latent and kinetic energy, and diabatic heating.

The thermodynamic equation, can be written in advective form as

$$c_p[\frac{\partial}{\partial t}T + \mathbf{v}.\nabla T + \omega(\frac{\partial}{\partial p}T - \kappa\frac{T}{p})] \quad = \quad Q_1 \qquad (1)$$

where $Q_1$ is the diabatic heating per unit mass, $T$ is temperature, $\mathbf{v}$ is the horizontal velocity, $\omega$ is the vertical $p$-velocity, $\kappa=R/c_p$ and $c_p$ is the specific heat at constant pressure. Another alternative is to express the thermodynamic equation in terms of potential temperature $\theta$

$$c_p[\frac{\partial}{\partial t}\theta + \mathbf{v}.\nabla\theta + \omega\frac{\partial}{\partial p}\theta] \quad = \quad Q_1(\frac{p_o}{p})^\kappa \qquad (2)$$

The apparent simplicity of this form is counterbalanced by the fact that $\theta$ increases with height nonlinearly and very rapidly in the lower stratosphere whereas the lapse rate for temperature is more nearly constant with height, with the main change at the tropopause. Hence finite differences (especially at coarse

vertical resolution) are much more accurate using the temperature form except perhaps at the tropopause. Nevertheless, these forms of the equations do not produce very accurate results when their vertical integrated $Q_1$ is compared with the correct result for the vertically-integrated equations.

Adding in the kinetic energy equation to (1) gives the total dry energy equation

$$\frac{\partial}{\partial t}(c_p T + k) + \mathbf{v}.\nabla(s+k) + \omega\frac{\partial}{\partial p}(s+k) = Q_1 - Q_f \quad (3a)$$

or in flux form

$$\frac{\partial}{\partial t}(c_p T + k) + \nabla\cdot(s+k)\mathbf{v} + \frac{\partial}{\partial p}(s+k)\omega = Q_1 - Q_f \quad (3b)$$

where $Q_f$ is the frictional heating arising from dissipation of kinetic energy (which is included in $Q_1$ but is very small (Li et al. 2007)), $k$ is the kinetic energy, and $s = c_pT+\Phi$ is the dry static energy. Although this is closest to an expression for the dry static energy equation, it includes the kinetic energy and the tendency term does not involve $s$.

The potential advantage of this form is that it avoids the difficulties associated with the static stability term in the thermodynamic equation that is related to the conversion of potential and internal energy into kinetic energy, and which is sensitive to small errors. The flux form (3b) involves convergence or divergence of $s+k$, and has some advantages such as vertical differencing that automatically cancels out terms and the vertical integral is easily satisfied. However, it requires very strict adherence to the equation of continuity being exactly satisfied. Finite differences have to be formulated so that identities such as

$$\omega\frac{\partial}{\partial p}T \quad = \quad \frac{\partial(\omega T)}{\partial p} - T\frac{\partial\omega}{\partial p}$$

hold, and this is readily done, as shown in Trenberth et al. (1995), but nevertheless is non-trivial. In particular, the same algorithms must be used as in formulating the equation of continuity and in evaluating $\omega$ and geopotential. In model coordinates, this is best done in the framework of the model used for data assimilation, which is not available. To ensure that the mass budget is balanced, we have previously mainly employed a barotropic correction to the divergent wind component, and this will still be employed. Then $\omega$ can be computed by integrating from either the bottom or the top of the atmosphere to the level of concern.

Vertically integrating (3b) gives

$$\frac{\partial}{\partial t}\frac{1}{g}\int_0^{p_s}(c_pT + k + \Phi_s)dp + \nabla.\frac{1}{g}\int_0^{p_s}(s+k)\mathbf{v}\,dp \quad = \quad \hat{Q}_1 - \hat{Q}_f \quad (4)$$

where lower boundary conditions are fully accounted for analytically and the ^ is the vertical integral.

We also use the conservation of moisture equation in advective form

$$\frac{\partial q}{\partial t} + \mathbf{v}.\nabla q + \omega\frac{\partial q}{\partial p} \quad = \quad e - c \quad (5)$$

where $q$ is the specific humidity, $e$ is the evaporation and $c$ the condensation. When vertically integrated, the latter give $E–P$ where $E$ is the surface evaporation and $P$ is the net surface precipitation rate. The whole equation can be expressed also in terms of energy by multiplying by $L$, the latent heat of vaporization. Frequently the term $Q_2 = L(c - e)$ is referred to as the apparent latent heating arising from the apparent moistening (see Trenberth (1997) for more details). The use of "apparent" here is because it includes all the small scale unresolved eddy effects as well. When the energy form is added to (3a) the equation becomes the equation for the transport of moist static energy plus kinetic energy $s + Lq + k$, although the evolution is of the total atmospheric energy

$A_E = c_pT + \Phi_s + k + Lq$ where $\Phi_s$ is the surface geopotential. Vertically integrated $\hat{Q}_2 = L(P-E)$.

In ERA-40 the coefficients $L$ and $c_p$ vary with temperature and moisture, but are set at a constant value for our calculations. We computed the monthly mean $L$ by taking the ratio of the surface latent heat to the evaporation and values vary by less than 2% except where snow exists, perhaps reflecting a contribution from ablation (solid to vapor).

From (3) we expect to be able to compute the diabatic heating and individual terms. The result is a new mapping of the atmospheric heat budget and exposition of the role of dynamical processes in the vertical temperature structure. If we set $T = \overline{T} + T'$, where the overbar is the time average and the prime is the departure, then we can also compute mean and transient eddy flux terms and (3a) becomes

$$\frac{\partial}{\partial t}(c_p\overline{T} + \overline{k}) + \overline{\mathbf{v}}.\nabla(\overline{s} + \overline{k}) + \overline{\omega}\frac{\partial}{\partial p}(\overline{s} + \overline{k}) +$$

$$\nabla.\overline{\mathbf{v}'(s'+k')} + \frac{\partial}{\partial p}\overline{(s'+k')\omega'} = \overline{Q}_1 - \overline{Q}_f \quad (6)$$

Similar expansions occur for the moisture equation (5) for which mass corrections are much less critical and, expressed in energy form, is

$$L\left[\frac{\partial\overline{q}}{\partial t} + \overline{\mathbf{v}}.\nabla\overline{q} + \overline{\omega}\frac{\partial\overline{q}}{\partial p} + \nabla.\overline{\mathbf{v}'q'} + \frac{\partial}{\partial p}\overline{q'\omega'}\right] = -\overline{Q}_2 \quad (7).$$

The sum of (6) and (7) gives the total energy equation for the atmosphere

$$\frac{\partial}{\partial t}(c_p\overline{T}+\overline{k}+L\overline{q})+\overline{\mathbf{v}}.\nabla(\overline{h}+\overline{k})+\overline{\omega}\frac{\partial}{\partial p}(\overline{h}+\overline{k})+$$

$$\nabla.\overline{\mathbf{v}'(h'+k')}+\frac{\partial}{\partial p}\overline{(h'+k')\omega'}=\overline{Q}_1-\overline{Q}_f-\overline{Q}_2 \qquad (8)$$

where $h = s+Lq$ is the moist static energy.

For the vertical integrals, $\hat{Q}_1$ is the sum of the downward net radiation at the TOA, the surface sensible and radiative heating, and the latent heating, plus any small scale effects. Consequently, $\hat{Q}_1-\hat{Q}_2$ is the sum of the TOA downward radiation plus the net upward surface fluxes, including the evaporative moistening flux *LE*. Therefore it is also the net radiative flux convergence, plus the sensible heating and latent energy moistening.

We have computed terms of the local temperature tendencies for monthly means as contributions from the terms in the above equation (8) and in particular divergences of fluxes by:

1. horizontal transient eddies of dry static energy, latent energy [e.g., terms involving fluxes $\overline{u'T'},\overline{v'T'},\overline{u'q'},\overline{v'q'},\overline{u'\Phi'},\overline{v'\Phi'}$ ]
2. transient eddies involving vertical transports [e.g., $\overline{\omega'T'},\overline{\omega'q'},\overline{\omega'\Phi'}$ ]
3. quasi-stationary components, horizontal transports [e.g., $\overline{v}\overline{T},\overline{v}\overline{q},\overline{v}\overline{\Phi}$ ]
4. quasi-stationary vertical transports (such as mean subsidence) [e.g., $\overline{\omega}\overline{T},\overline{\omega}\overline{q},\overline{\omega}\overline{\Phi}$ ].
5. tendency (storage) terms.
6. mean apparent diabatic heating, $\overline{Q_1}$
7. mean apparent latent heating, $\overline{Q_2}=L(\overline{P}-\overline{E})$ .

The tendency terms are computed from the difference between the value at the end of the month minus that at the beginning of the month, interpolated to the correct time of 2100 UTC prior to the first analysis time of each month. However, the tendency terms are given in Trenberth et al. (2002a) and will not be presented here. The size of the tendency terms reflects the synoptic variability, which averages out over longer times. The $Q_1$ and $Q_2$ terms are computed as residuals from the heat and moisture equations and include contributions from small-scale unresolved processes. These will apply to layers.

We can also compute the atmospheric forcing terms $Q_1$, $Q_2$ and $Q_1$-$Q_2$ from model results. In the case of the ERA-40 reanalyses, the three dimensional fields of the components of these quantities are not available. However the vertical integrals are. They can be computed as follows:

$$\hat{Q}_1 = R + SH + LP \qquad (9)$$

$$\hat{Q}_2 = L(P-E) \qquad (10)$$

$$\hat{Q}_1-\hat{Q}_2 = R + SH + LE \qquad (11)$$

Where *R* is the net radiation convergence and is made up of the solar and long-wave components, and *SH* is the surface sensible heat. The archive has the surface sensible and latent heat fluxes as well as surface and TOA radiation in solar and thermal bands. These are accumulated fields based on the assimilating model parameterizations and physics, and have an advantage in that they do not suffer from temporal sampling, but the disadvantage in that they are not observed quantities.

## 3. Results

*a. Vertical integrals*

Computational results for January 1989 of the vertically-integrated diabatic heating, $Q_1 - Q_f$, are shown in Fig. 1 using the exact vertical integral in full model coordinates from (4) versus the results from (3a) or equivalently (6). Zonal means are shown in the right panels and the plots are truncated to T42 resolution. As the frictional component $Q_f$ is order 2 W m$^{-2}$ (Li et al. 2007) we interpret $Q_1 - Q_f$ for the most part as $Q_1$. Although the patterns from Fig. 1b are very similar in most respects to Fig. 1a, zonal mean rms differences are typically about 25 W m$^{-2}$ but increase to 35 W m$^{-2}$ near the equator and north of 60ºN. This provides a fundamental limitation on the accuracy of the results using pressure coordinates and this methodology.

We also examined the vertical integral from all the layers in (3b) via two different methods. Both methods mask data below ground in high topography regions but in different order. In the first method data were masked below ground by comparing the pressure level to surface pressure before computing vertical integrals and the divergences. This was also done conservatively by extending the mask to regions in the horizontal and vertical influenced by the ground. In method 2, divergences were first computed on levels and then areas below ground were masked using the surface pressure in computing vertical integrals. Only the second method enables the vertical structure to be examined, but evidently contamination from below-ground values is large. Neither produced acceptable results, as differences with the full model coordinate integral are on the order of several hundred W m$^{-2}$. Even in the first method, problems with mass balance and its correction, and how $\omega$ is computed arise as major issues, and many tests failed to produce acceptable results. Thus we focus on the advective form for the remainder of this study.

The various terms, vertically integrated, that contribute to $Q_1$ (Fig. 2) reveal that the main contributions come from the monthly mean advection terms while the transients contribute most in the extratropics and, not unexpectedly, are strongest in the winter hemisphere over the oceans in association with the storm tracks.

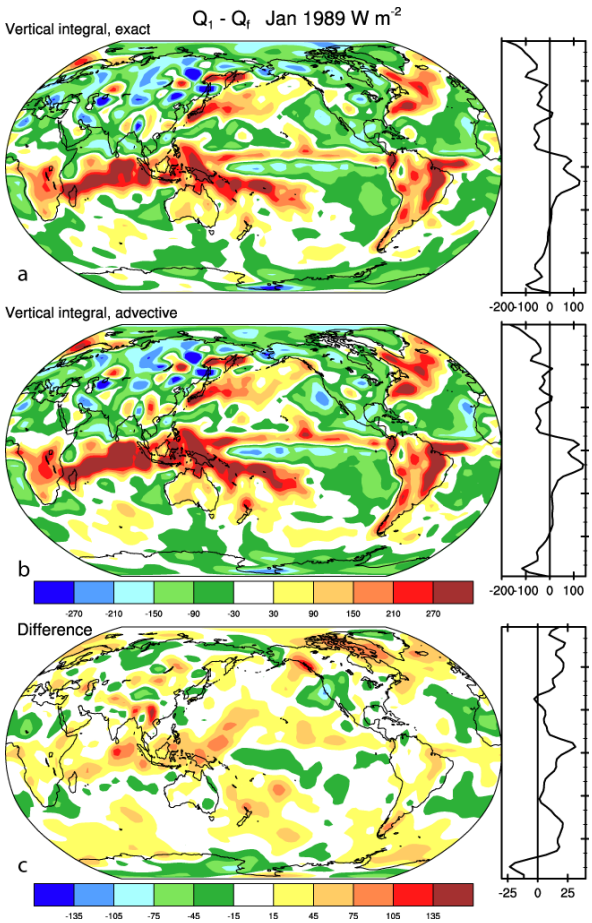


Fig. 1. For Jan 1989 based on ERA-40 analyses, (a) vertically integrated $Q_1 - Q_f$ truth (total vertically integrated from (4)), vs (b) results from the advective method (3a), and (c) differences between the two. The right hand side panels show the zonal averages. The plots are smoothed to T42 resolution and the units are W m$^{-2}$.

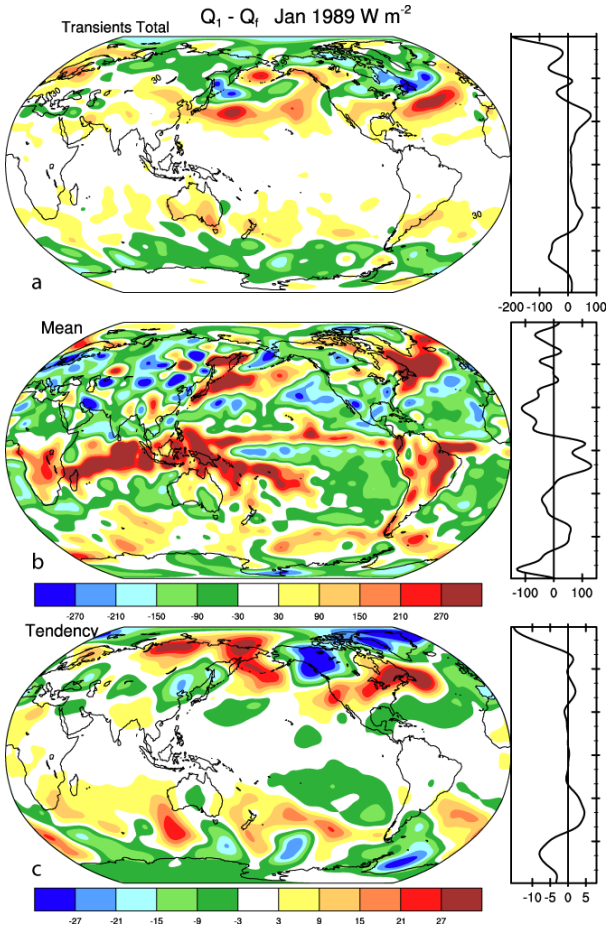


Fig 2. Vertically integrated contributions to $Q_1$-$Q_f$ from the (a) transient terms, (b) mean terms (same color key), and (c) tendency (color key units a factor of 10 less).

The tendency term for this month (Fig. 2c) contributes up to about 50 W m$^{-2}$, and is fairly small but not negligible. The mean vertical advection terms dominate overall, especially throughout the tropics, but in the northern hemisphere, where strong stationary waves are present, the mean horizontal and vertical advection terms are large but compensate one another. For instance warming over the eastern North Pacific is compensated for by cooling from upward motions, while the reverse occurs over eastern Siberia and Japan. The transient fluxes of energy result in cooling to the south and warming to the north of the storm tracks in the North Atlantic and Pacific for the horizontal component.

Figure 3 presents the vertically integrated contributions to $Q_1$-$Q_f$ from the horizontal advection ($\mathbf{v}.\nabla(s+k)$) and vertical advection ($\omega\partial(s+k)/\partial p$) terms as components from the monthly mean, within-month transients, and their sum. In this presentation the transients are the differences between the total and the mean terms, and thus depict the transient advection terms (as opposed to the flux terms in (6) and (8)). The transients relate to the storm tracks in mid-latitudes, and although relatively small, their systematic nature makes them important contributors to moving energy around. In particular, the transient vertical advection is negative, indicating systematic upward transport of energy, with largest values in the baroclinic storm tracks. This transport is compensated for by quasi-horizontal energy transport and radiative cooling for the most part.

Figure 4a presents $L(E-P) = -Q_2$ in W m$^{-2}$, which can be converted to give $E$-$P$ units of mm/day by dividing by a factor of 29. In this case we show only one version, as this field is much less sensitive to the computational methods and dry air mass conservation. Note how there is strong cancellation between $Q_1$ (Fig. 1) and $Q_2$ (Fig. 4a) as latent heat is realized and converted to dry static energy. Hence their combination on the right hand side of (8), $Q_1$-$Q_2$ (Fig. 4b), has less structure as the computed forcing of the total energy mostly has the moistening of the

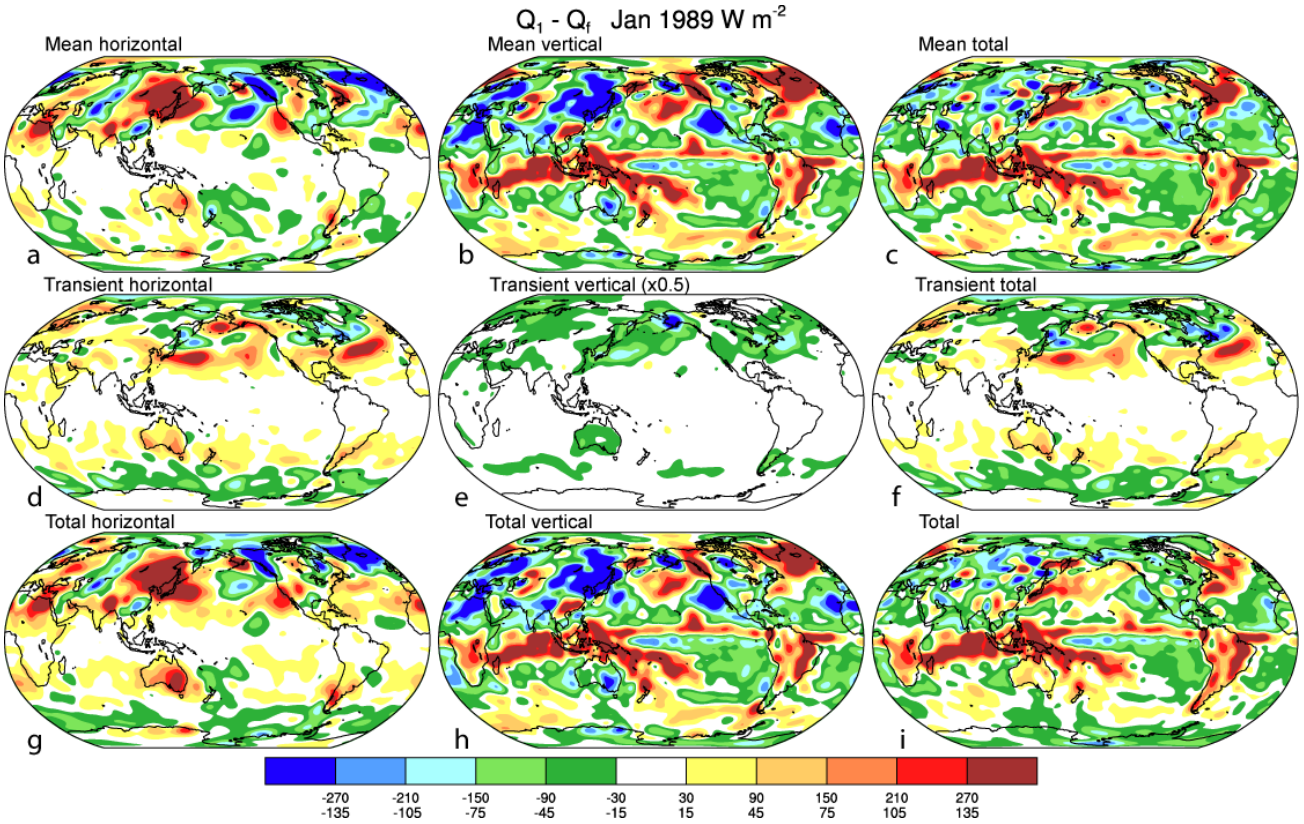


Fig 3. Vertically integrated components of Fig. 1b from the horizontal advection (left: a,d,g) and vertical advection (b, e, h), and from the mean terms (top: a, b, c) and the transients (middle: d, e, f), with the total (bottom: g, h, i). The upper scale on the color bar applies to all plots except for (e) where the color bar has half the contour interval of the other plots (lower scale).

atmosphere as a component but no latent heat component. However, there is a clear residual of the precipitation patterns in the $Q_1$-$Q_2$ map, reflecting the evaporative sources of moisture and cloud effects, although some of these may be corrupted by the lack of conservation of moisture in the reanalyses (Trenberth et al. 2007), as is especially evident over land masses such as Australia, that appear to (incorrectly) be moisture sources.

*b. Vertical structure*

The heat budget naturally involves vertical integration over a finite layer rather than depicting point values. One way to remove this layer dependence is to express results as an effective heating rate as a tendency of temperature in K per day. Thus the terms in Eq. (3a), for example, are expressed in terms of the first term divided by the specific heat. Another approach for cross sections is to express the energy as for a standard layer of, say, 100 hPa thickness. However, in cross sections the usual coordinate is one that is more nearly linear in height. Therefore in order to be able to readily assess layer contributions to the vertical integral, we have used a $Z = H \ln (p_o/p)$ coordinate, where $H$ is the scale height set at 7316 m corresponding to an

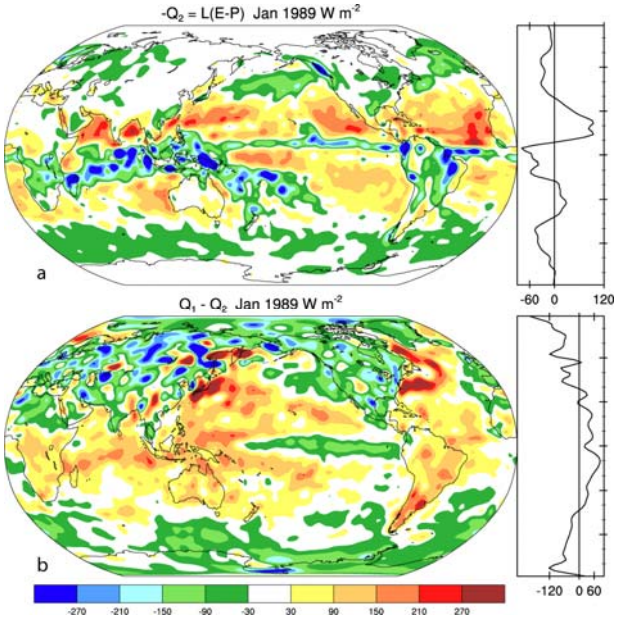


Fig. 4. The latent heating term $-Q_2=L(E-P)$ (a) and total heating (including moistening) $Q_1$-$Q_2$ (b) in W m$^{-2}$.

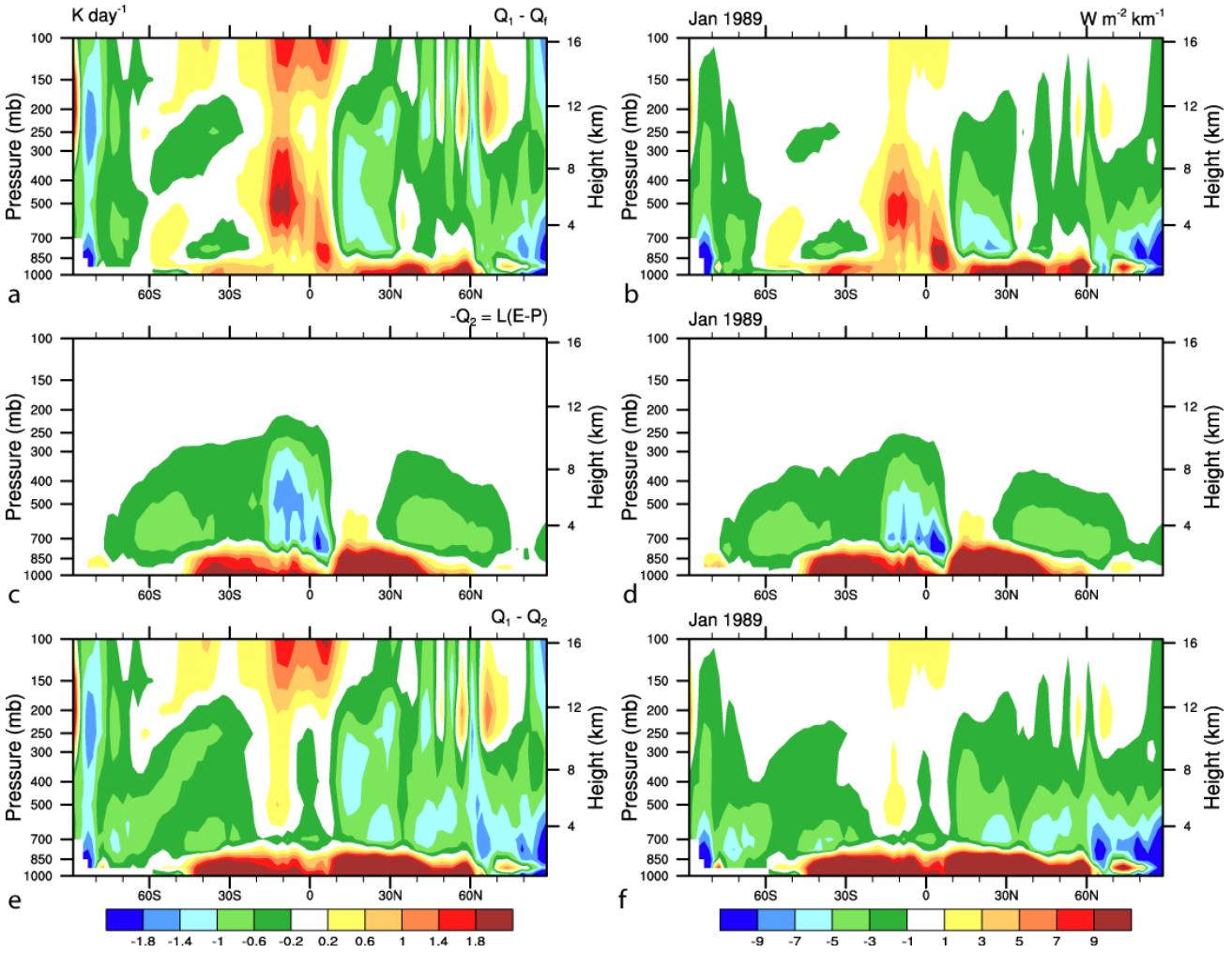


Fig. 5. The contributions as the zonal mean for January 1989 to $Q_1$, top (a, b), $Q_2$, center (c, d), and $Q_1 - Q_2$ bottom (e, f), as deduced from the dry, moist and total energy equations based on the tendencies and the three dimensional advection, and expressed as the temperature tendency K day$^{-1}$ on the left, and as a heating per km layer (W m$^{-2}$ km$^{-1}$) at right. The red areas are where there is divergence stemming from large surface evaporation in (c, d) or diabatic heating in (a, b) (often associated with latent heat release from moisture convergence and precipitation) transported vertically and horizontally, and the blue areas are those where energy converges as a result of precipitation (c, d) or cooling (a, b). In (e, f) these compensate each other and the main signature is the surface moistening and gain of latent energy, along with some sensible heating, and the pervasive radiative cooling above the boundary layer that is strongest in the winter hemisphere.

atmosphere with temperature of 250 K, and units are then W m$^{-2}$ per kilometer.

The zonal average cross sections up to 100 hPa (Fig. 5) have the two different units for comparison and the 3 panels show $Q_1$, $Q_2$ and $Q_1$-$Q_2$. The left panels (a, c, e) are in K day$^{-1}$ and reveal a lot more of the heating rates in the upper troposphere and lower stratosphere that otherwise contribute relatively little to the total, as seen in the right panels (b, d, f) which have units of W m$^{-2}$ km$^{-1}$. In the lower troposphere, roughly 0.2 K day$^{-1}$ corresponds to about 1 W m$^{-2}$ km$^{-1}$. The right panels are easier to interpret as different parts of the figure are more readily quantitatively compared owing to the mass weighting.

Figure 5c,d clearly show the main precipitation and associated latent heat release nearly everywhere above the boundary layer. The combination of the Intertropical Convergence Zone (ITCZ), South Pacific Convergence Zone (SPCZ) and monsoon trough rains are strongly evident from 10°N to 16°S. The mid-latitude storm tracks are also clearly evident. At and near the surface, evaporation and moistening of the atmosphere dominates along with small-scale mixing through the mixed layer, especially in the subtropics. The rainfall is reflected in the top left panel (Fig. 5a) as the dominant diabatic heating source. The third row (Fig. 5e, f) again reflects the moistening in the mixed layer but cancellation of the latent

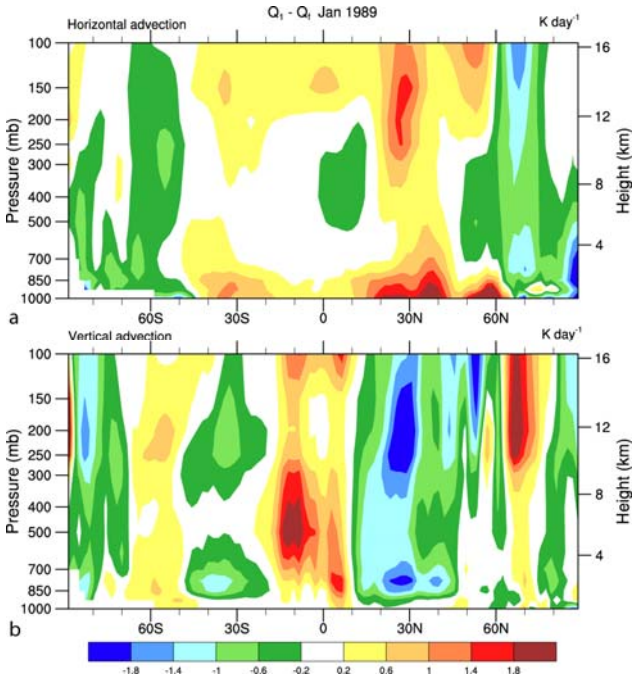


Fig. 6 Vertical cross section of contributions to total diabatic heating from the horizontal (top) and vertical (bottom) advection terms in K day$^{-1}$. Warm (cold) colors signify dynamic cooling (heating) that is compensated for by either diabatic heating (cooling) or other dynamic processes (note the cancellation between the two panels).

heat component. In Fig. 5e, f cooling dominates in the regions above the mixed layer, presumably mainly arising from radiative cooling that is strongest in the northern (winter) hemisphere. Whether the weak band of heating near 10°S is from convective (small scale) heating or reflects lack of conservation of energy or moisture in the analyses arising, for instance, from increments in the analyses, is difficult to say. The main differences between the two units (a, c, e versus b, d, f) are above about 300 hPa in the tropics where heating rates of over 1.5 K day $^{-1}$ are found. These may be associated with ozone radiative heating.

The zonal average cross sections of the main contributing terms for advection in the horizontal $\mathbf{v}.\nabla(s+k)$ and vertical $\omega\partial(s+k)/\partial p$ (Fig. 6) thus reveal the main processes that compensate for $Q_1$. Here the units of K day$^{-1}$ are shown to reveal aspects of the vertical structure in the upper troposphere and lower stratosphere that do not contribute significantly to the vertical integral. The horizontal advection compensates for cooling at high latitudes in the troposphere, and heating in mid-latitudes in the lower troposphere. In fact this pattern extends well into the stratosphere consistent with the baroclinic nature of the planetary waves in the northern hemisphere winter. In contrast, the vertical advection term compensates for heating in the tropics and cooling in the subtropics as major drivers of the Hadley circulation. Poleward of 20° these terms cancel to some extent in the total $Q_1$ field (Fig. 6b), as horizontal advective cooling helps drive the subsidence in the downward branch of the Hadley circulation (Trenberth and Stepaniak 2003b).

Maps of layers of $Q_1$ are shown in Fig. 7 for 300 to 100 hPa, 850 to 300 hPa, and surface to 850 hPa. In the tropics, both top layers are in the troposphere and they are clearly similar. In the extratropics, the top layer is largely in the lower stratosphere and it is quite noisy over land. Biggest differences with the main tropospheric layer occur over the oceans where there is also a connection to the surface layer that is much more obviously related to surface fluxes of sensible and latent heat, as cold and dry air comes off the east coast of Asia and North America. The cooling over northern land masses is most prevalent in the middle layer.

The vertical fluxes of energy $\omega(s+k)$ at 500 hPa (Fig. 8) are dominated by the mean term (not shown), although upward transport of energy is clearly identified with the storm tracks in both hemispheres

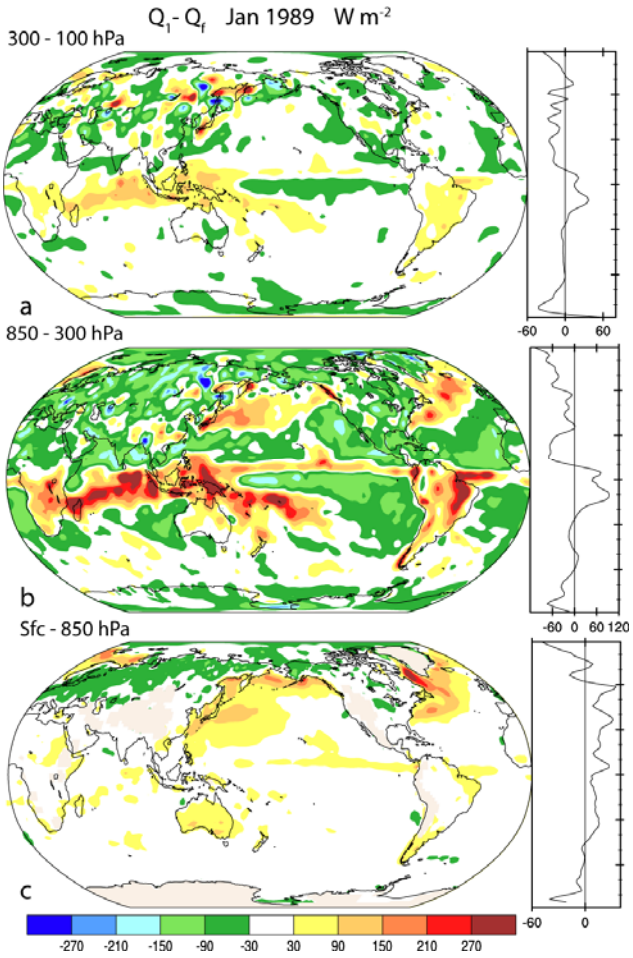


Fig. 7. Contributions to the total diabatic heating for the surface to 850 (c), 850 to 300 (b) and 300 to 100 hPa (a) layers in W m$^{-2}$.

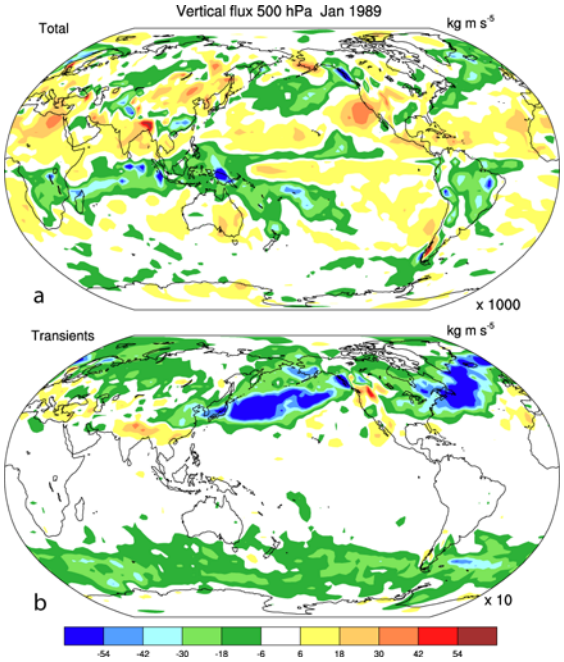


Fig. 8. The vertical flux of energy as $\omega(s+k)$ for the total (a) and transient terms (b) but with the units of kg m $s^{-5}$ multiplied by 1000 (a) and 10 (b), so that the monthly mean term dominates and looks just like the top panel. Negative values signify upward transport of energy by the flow.

in the transient terms (Fig. 8b). Patterns and magnitudes are quite similar at 850 and 300 hPa (not shown) although the transient component is much weaker at 300 hPa. Over the eastern tropical Pacific, the ITCZ is much more active at 850 (not shown) than 500 hPa (Fig. 8), highlighting its different vertical structure (Trenberth et al. 2000). The size of the mean term, being a factor of 100 greater than the transient term, does not mean it is more important by this amount. The mean value of $s$ is large and positive, so the pattern simply shows the ω field. But it is only its vertical gradients that matter for the vertical transports, as mean part of the vertical flux is canceled by the horizontal flux through conservation of mass (i.e. $s(\nabla.\mathbf{v} + \partial\omega/\partial p) = 0$).

The vertically integrated quasi-horizontal flux of $\mathbf{v}(s+k)$ (Fig. 9) reveals strong meridional transports centered on the storm tracks in each hemisphere, while the divergence pattern shows the dipole structure with the zero point slightly on the equatorwards side of the vertical fluxes at 500 hPa (Fig. 8). Trenberth (1991b) showed that $v'T'$ and $\omega'T'$ have similar profiles across a storm track, with peak values centered on the storm track, as expected for baroclinic eddies.

For the moist component, $L(E-P) = -Q_2$ (Fig. 4a), the vertical structure by layer (Fig. 10) confirms the small contributions above 300 hPa, but with striking differences above and below 850 hPa. In the troposphere, the dominance of latent heating in precipitation is

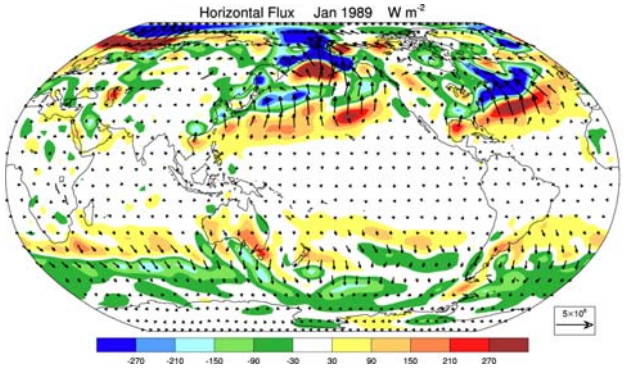


Fig. 9. Vertically integrated horizontal flux of dry energy $(s+k)$ as vectors (scale arrow lower right in W $m^{-1}$), and its divergence in W $m^{-2}$ as color contours.

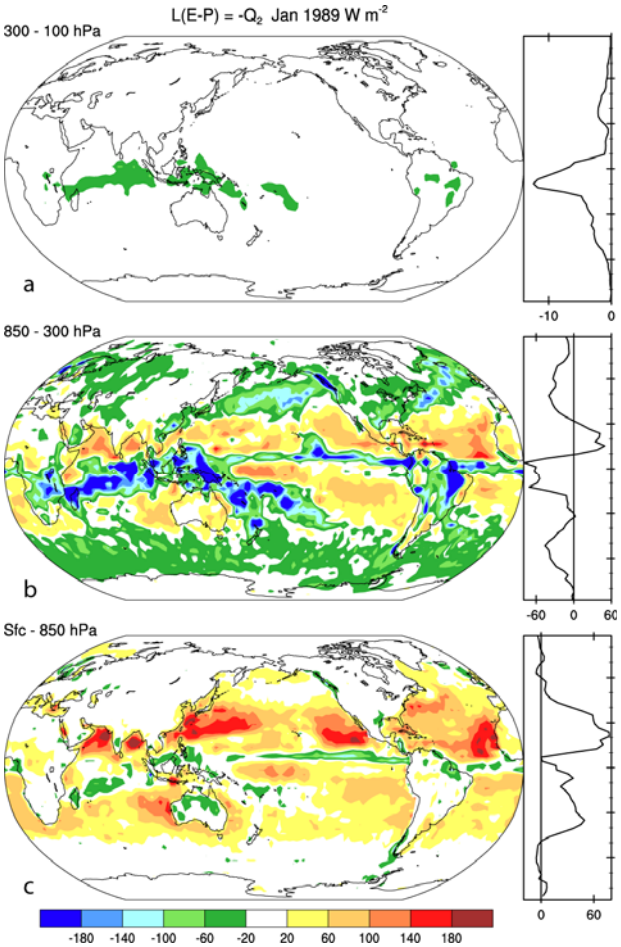


Fig. 10. Contributions to the total latent heating $(L(E-P))$ for the (c) surface to 850, (b) 850 to 300 and (a) 300 to 100 hPa layers in W $m^{-2}$. Warm colors indicate moistening, and cold colors indicate precipitation.

emphasized, although with the dry areas showing positive values, implying sources of moisture. The latter are clearly evident below 850 hPa in the subtropics,

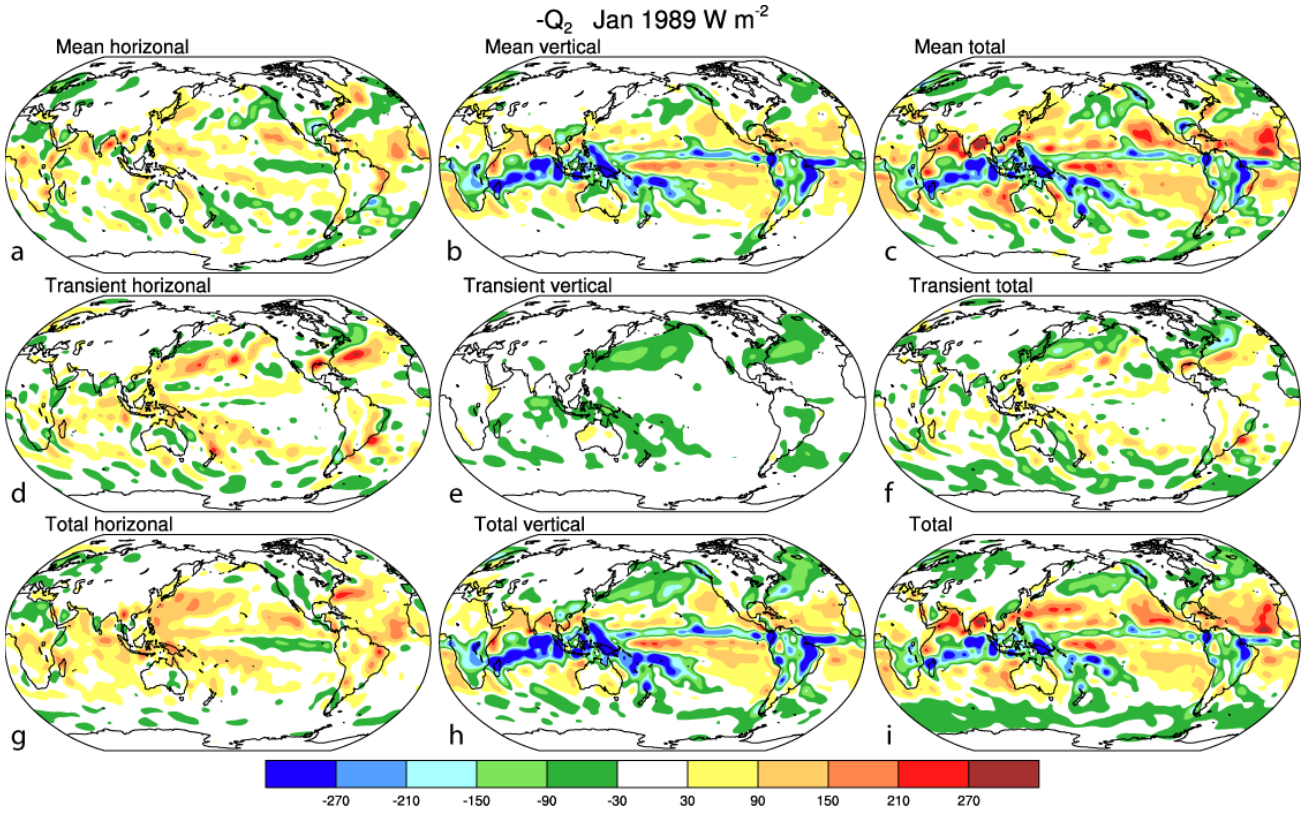


Fig. 11. Contributions to the total latent heating (*L(E-P)*) for horizontal (left: a, d, g) and vertical (b, e, h) advection and their sum (right: c, f, i), for the monthly mean (top: a, b, c), transients (middle: d, e, f) and the total (bottom: g, h, i) in W $m^{-2}$. Warm colors indicate drying by the dynamics of moisture transport and thus moistening by other terms, and cold colors indicate precipitation and latent heat release.

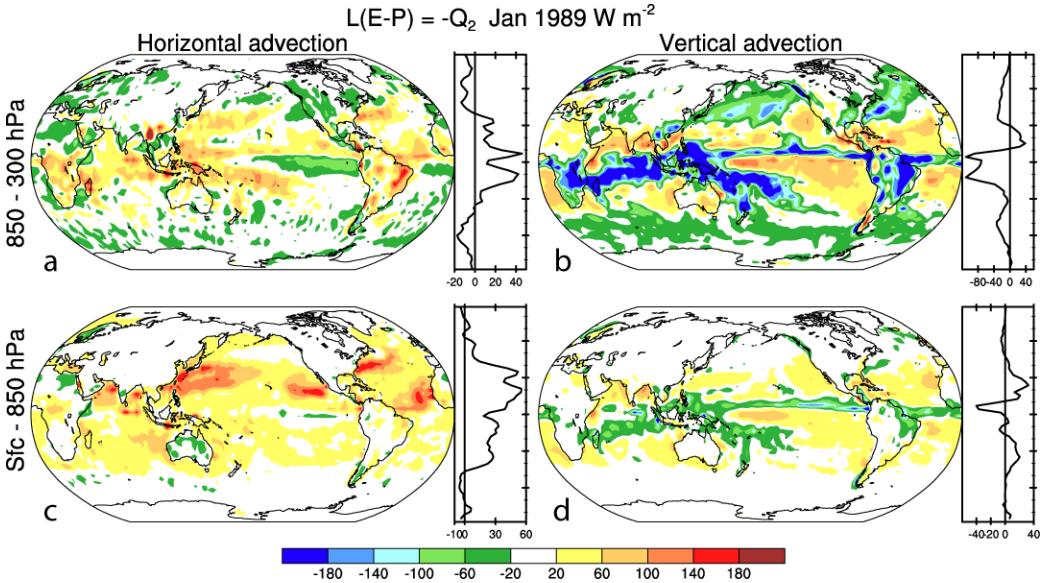


Fig. 12. Contributions to the total latent heating (*L(E-P)*) for horizontal (a, c) and vertical (b, d) advection for the layers (c, d) surface to 850 hPa and (a, b) 850 to 300 hPa in W $m^{-2}$. Warm colors indicate drying by the dynamics of moisture transport and thus moistening by other terms, and cold colors indicate moisture convergence and thus precipitation and latent heat release. Horizontal moisture transport feeds the vertical moisture advection that results in precipitation.

especially, where maximum surface evaporation is known to occur, but its extension above 850 hPa is a bit surprising. In Fig. 5c,d we see that it does not extend much above 850 hPa. As it is computed from the dynamics terms, it really means there are moisture transports away from those regions, implying evaporation or subgrid-scale mixing to provide the moisture source.

Examining the mean and transient contributions to the moisture fluxes that result in evaporation or precipitation shows that the mean terms strongly dominate the transient terms (Fig 11). Figure 11 also shows the contributions from the horizontal and vertical advection terms. The moisture fields are dominated by the monthly mean terms and the transient contributions are small. The vertical advection term dominates (Fig. 11) throughout the tropics, where it directly relates to precipitation, although partially compensated for by horizontal moisture advection and thus convergence. The latter is mainly in the boundary layer below 850 hPa (not shown).

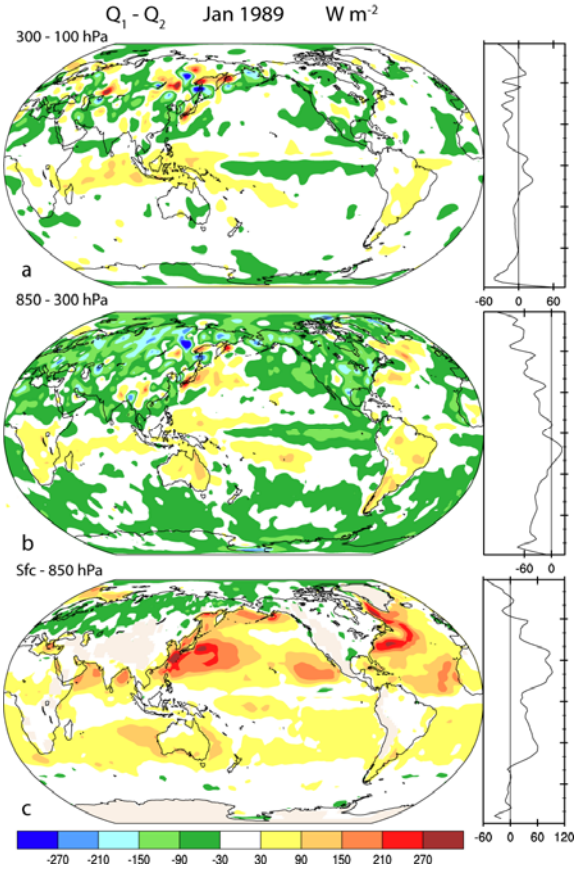


Fig. 13. Contributions to the total energy $Q_1$-$Q_2$ for the layers (c) surface to 850, (b) 850 to 300 and (a) 300 to 100 hPa in W m$^{-2}$.

The horizontal and vertical moisture advective terms below 300 hPa (Fig. 12) show the transports in the boundary layer especially, as moisture is transported equatorward towards the ITCZ, and poleward towards the extratropical storms tracks. The tendency terms are all small (not shown). Hence surface evaporation supplies the moisture that is transported horizontally and feeds the vertical moisture advection resulting in precipitation.

For $Q_1$-$Q_2$, there is a great deal of cancellation in the vertical integral as latent heating is realized as dry static energy, and this cancellation is further illustrated for layers in Figure 13. Both the lower stratosphere, 300 to 100 hPa, and the troposphere, 850 to 300 hPa maps are rather noisy. The boundary layer, surface to 850 hPa (Fig. 13c), illustrates strong heating off the eastern coasts of Asia and North America. The northern continents are the main source of cooling, presumably radiative, while the southern hemisphere continents feature net heating. Part of this may be sensible heating and associated dry convection. However, even for the 300 to 100 hPa layer there is a signature of tropical convection over the oceans, with the ITCZ, SPCZ and Walker circulation downward branch signatures clearly evident.

*c. Atmospheric forcings*

To complement the diagnostics shown here, and help with the interpretation, we also present the direct computation of $Q_1$, $Q_2$ and $Q_1$-$Q_2$ from the model fields in the reanalyses, as well as some of the components where we can assess their accuracy. The vertical integrals are given in Fig. 14 along with their differences with the corresponding fields in Figs. 1a and 4. The fields are quite similar overall, although with much less small-scale structure over land, and also with some large-scale differences that are substantial. These can be traced for the most part to model biases and known problems with the ERA-40 fields (Fig. 15).

To help establish these aspects, we therefore present (Fig. 15a) the precipitation from the model and (Fig. 15d) differences from the Global Precipitation Climatology Project (GPCP) (Adler et al. 2003). Also shown are TOA radiation for the absorbed solar radiation (ASR) (Fig. 15b) and outgoing longwave radiation (OLR) (Fig. 15c) components and differences with Earth Radiation Budget Experiment (ERBE) (Trenberth 1997) data (Fig. 15e, f). The well known overestimate of tropical precipitation (Uppala et al. 2005; Trenberth et al. 2007) shows up as excess latent heating of 30 to 200 W m$^{-2}$ and with zonal average differences of 3 mm/day (90 W m$^{-2}$) at 7ºN. There are also biases in location as the SPCZ is shifted north, leaving large negative biases, up to 7 mm/day (210 W m$^{-2}$), over especially the southwest Pacific, and zonal mean negative biases of -30 W m$^{-2}$ at 40ºS. Comparable negative biases exist regionally in the northern extratropics. Globally the bias in precipitation in ERA-40 model values is 0.39 mm/day (11.4 W m$^{-2}$).

Although much of the bias in $Q_2$ (Fig. 14e) is traceable to the precipitation field, the pattern is not the same and one interpretation is that evaporation biases also exist. Trenberth et al. (2007) indeed confirm biases in

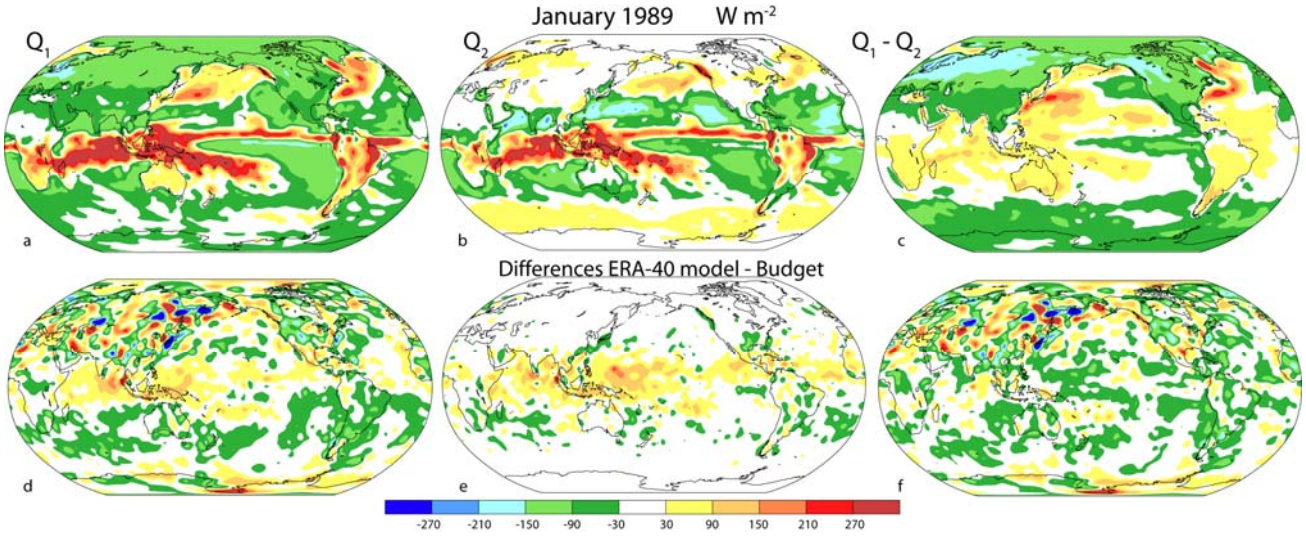


Fig. 14. (a) $Q_1$, *(b)* $Q_2$ and (c) $Q_1$-$Q_2$ estimated directly from (9), (10), and (11) from the model accumulated values and their differences (d, e, f) with the vertically-integrated budget derived quantities in Figs. 1a and 4.

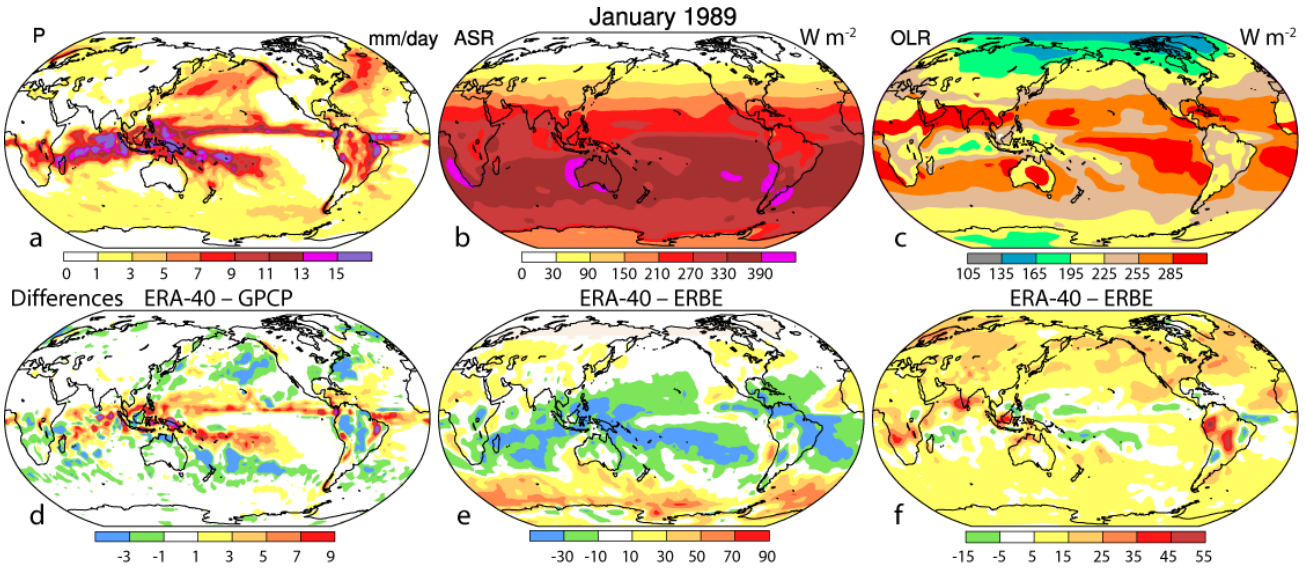


Fig. 15. Estimates for January 1989 of precipitation in mm/day (a), and ASR (b), and OLR (c) in W m$^{-2}$ from ERA-40 based on accumulated model fields (top: a, b, c) and differences (below: d, e, f) with (d) GPCP, and (e, f) ERBE.

evaporation over land in ERA-40 reanalyses associated with spurious sources of moisture and excess evaporation, but these also affect $Q_2$. As the model $Q_2$ has a global mean of 9.5 W m$^{-2}$ whereas the global mean tendency in moisture storage is 0.15 W m$^{-2}$, the model value is biased high by 9.4 W m$^{-2}$. Hence much of the differences in $Q_2$ estimates are accounted for as model bias.

Substantial biases also exist in radiation fields. The OLR (directed up) is too large in the ERA-40 model almost everywhere except in the deep convection regions, with biases of 5 to 30 W m$^{-2}$. The solar radiation biases are much greater and negative in the tropics (too much cloud or cloud that is too bright) and positive over the southern oceans (not enough cloud), with biases of order 50 W m$^{-2}$ in both regions. Uppala et al. (2005) note that there is an imbalance of -7 W m$^{-2}$ overall in ERA-40 and this is ascribed in part to over-reflective cirrus clouds. Globally the biases in ASR and OLR in Fig. 15e,f are -2.2 and 9.4 W m$^{-2}$, with an overall bias in net radiation of 7.3 W m$^{-2}$ cooling.

The observed tendency in global mean $Q_1$ (Fig. 2c) is 0.08 W m$^{-2}$, while the global mean model $Q_1$ has a

tendency of -3.5 W $m^{-2}$ in spite of a 9.4 W $m^{-2}$ bias contribution from latent heat. These suggest that the global means of sensible heat of 13.6 W $m^{-2}$ plus radiation of -107.0 W $m^{-2}$ are biased by -12.9 W $m^{-2}$, and so this emphasizes a strong negative bias in radiative cooling, as the expected error in *SH* is only order 2 W $m^{-2}$. Indeed for $Q_1$-$Q_2$, coming from the sum of radiation and surface fluxes of sensible and evaporative latent heat, the global mean bias is -13.0 W $m^{-2}$. Hence much of the large scale structure in the difference panels of Fig. 14 can be traced to model biases. The small-scale structure in results from the budget calculations relates to the divergence term but is less evident in the model forcings.

## 4. Discussion and conclusions

In this paper, we document an approach to diagnosing the moistening and diabatic heating of the atmosphere based upon the dry energy and moisture equations and their combination for the total energy. The method is applied to the ERA-40 reanalyses which have sufficient problems in both the temperature (Trenberth and Smith 2006) and moisture (Trenberth et al. 2005) fields that the results can not be taken as definitive. Extensive tests were performed to see how well the vertical structure could be elucidated given the constraint of satisfying the vertical integral, which is known from analytical integration. The methods involving the flux formulation of the equations are prone to considerable errors owing to lack of conservation of mass and violation of other numerical identities that occurs when variables are interpolated onto pressure coordinates. An advective formulation produces reasonable results, with local errors of order 25 W $m^{-2}$ for the vertical integral. Similar computations in a model framework show that accurate results are only possible when all of the numerical discretization used in the model is also applied for the diagnostics. But some results are more robust to methods than others.

However, pressure coordinates are essential in order to be able to compare results from all the different model and analysis coordinates. Higher resolution (of order 40 model levels with 25 or 50 hPa resolution in the troposphere) than that in the older archives (typically 17 model levels) is also highly desirable. This would allow the vertical structure to be better depicted and more accurate numerical results to be computed.

An analysis of the atmospheric forcings as computed from the assimilating ERA-40 model reveals significant biases when compared with observations and these biases are reflected in the differences computed with the budget-derived quantities, suggesting that the latter are more reliable. However, only their sum can be computed from the energy and moisture budgets and the model-derived fields can provide extra information to aid in interpretation.

Even with the known shortcomings in the analyses, and the fact that they do not conserve moisture or energy owing to the analysis increments, many of the budget-derived fields and cross sections seem physically reasonable and can be interpreted in terms of the known diabatic processes. For instance, surface evaporation moistens the boundary layer and results in moisture being transported quasi-horizontally to convergence regions such as the ITCZ, SPCZ and monsoon troughs where it is precipitated out. Transient disturbances play a more important role in the extratropical storm tracks, but even there the monthly mean flow transports and divergence appear to be more important. The latent heat realized dominates the diabatic heating field, and radiative cooling dominates the tropospheric diabatic cooling. Ozone heating may be the source of the heating near 100 hPa in the tropics.

We plan to apply the methods outlined here to analyses and model results as diagnostics. To the extent that we can believe the analyses, the results provide checks on the model results. However, the main use to be made of the diagnostics is to explore the static stability of the atmosphere and how it is maintained, by examining all months and years for reanalyses after 1979. Atmospheric models typically suggest increasing temperature increases with height in the tropics, following the saturated adiabatic lapse rate (IPCC 2007). We hope to shed some light on how realistic this may be.

**Acknowledgements** This research is partially sponsored by the NOAA CCDD and CLIVAR programs under grants NA04OAR4310073 and NA06OAR4310145.

**References**

Adler RF, Huffman GJ, Chang A, Ferraro R, Xie P,. Janowiak J, Rudolf B, Schneider U, Curtis S, Bolvin D, Gruber A, Susskind J, Arkin P, Nelkin E (2003) The version 2 Global Precipitation Climatology Project (GPCP) monthly precipitation analysis (1979–present). J Hydrometeor 4 1147–1167

Boville BA (1985) The thermal balance of the NCAR Community Climate Model. J Atmos Sci 42: 695-709

Fasullo JT, Trenberth KE (2008a) The annual cycle of the energy budget: Global mean and land-ocean exchanges. J. Climate 21: in press

Fasullo JT, Trenberth KE (2008b) The annual cycle of the energy budget: Meridional structures and poleward transports. J. Climate 21: in press

Hoskins BJ, Sardeshmukh PD (1987) A diagnostic study of the dynamics of the Northern Hemisphere winter of 1985-86. Quart J Roy Meteorol Soc 113: 759-778

IPCC (2007) Climate Change 2007. The Physical Science Basis. Contribution of WG 1 to the Fourth Assessment Report of the Intergovernmental Panel on Climate Change. Solomon S, Qin D, Manning M, Chen Z, Marquis MC, Averyt KB, Tignor M, Miller HL (eds). Cambridge University Press. Cambridge, UK., and New York, NY, USA, 996 pp.

Johnson RH, Ciesielski PE (2000) Rainfall and radiative heating rates from TOGA COARE atmospheric budgets. J Atmos Sci 57: 1497-1514

Li L, Ingersoll AP, Jiang X, Feldman D, Yung Y (2007) Lorenz energy cycle of the global atmosphere based on reanalysis datasets. Geophys Res Lett 34: L16813, DOI10.1029/2007GL029985

Tian B, Zhang GJ, Ramanathan V (2001) Heat balance in the Pacific Warm Pool atmosphere during TOGA COARE and CEPEX. J Climate 14: 1881-1893

Trenberth KE (1991a) Climate diagnostics from global analyses: Conservation of mass in ECMWF analyses. J Climate 4: 707–722

Trenberth KE (1991b) Storm tracks in the southern hemisphere. J Atmos Sci 48: 2159–2178

Trenberth KE (1997) Using atmospheric budgets as a constraint on surface fluxes. J Climate 10: 2796–2809

Trenberth KE, Fasullo J (2008) An observational estimate of ocean energy divergence. J Phys Oceanogr in press

Trenberth KE, Smith L (2006) The vertical structure of temperature in the tropics: Different flavors of El Niño. J Climate 19: 4956–4970

Trenberth KE, Stepaniak DP (2002) A pathological problem with NCEP reanalyses in the stratosphere. J Climate 15: 690–695

Trenberth KE, Stepaniak DP (2003a) Co-variability of components of poleward atmospheric energy transports on seasonal and interannual timescales. J Climate 16: 3691-3705

Trenberth KE, Stepaniak DP (2003b) Seamless poleward atmospheric energy transports and implications for the Hadley circulation. J Climate 16: 3706-3722

Trenberth KE, Stepaniak DP (2004) The flow of energy through the Earth's climate system. 2004. Quart J Roy Meteor Soc 130: 2677–2701

Trenberth KE, Caron JM, Stepaniak DP (2001) The atmospheric energy budget and implications for surface fluxes and ocean heat transports. Clim Dyn 17: 259-276

Trenberth KE, Fasullo J, Smith L (2005) Trends and variability in column-integrated water vapor. Clim Dyn 24: 741-758

Trenberth, KE, Hurrell, JW, Solomon A (1995) Conservation of mass in three dimensions, J Climate 8: 692-708.

Trenberth KE, Stepaniak DP, Caron JM (2000) The global monsoon as seen through the divergent atmospheric circulation. J Climate 13: 3969–3993

Trenberth KE, Stepaniak DP, Caron JM (2002a) Accuracy of atmospheric energy budgets from analyses. J Climate 15: 3343-3360.

Trenberth KE, Stepaniak DP, Caron JM (2002b) Interannual variations in the atmospheric heat budget. J Geophys Res 107 D8 DOI 10.1029/2000JD000297

Trenberth KE, Caron JM, Stepaniak DP, Worley S (2002c) The evolution of El Niño Southern Oscillation and global atmospheric surface temperatures. J Geophys Res 107 D8 DOI 10.1029/2000JD000298

Trenberth KE., Smith L, Qian T, Dai A, Fasullo J (2007) Estimates of the global water budget and its annual cycle using observational and model data. J Hydrometeor 8: 758–769

Uppala SM, Kållberg PW, Simmons AJ, Andrae U, da Costa Bechtold V, Fiorino M, Gibson JK, Haseler J, Hernandez A, Kelly GA, Li X, Onogi K, Saarinen S, Sokka N, Allan RP, Andersson E, Arpe K, Balmaseda MA, Beljaars ACM, van de Berg L, Bidlot J, Bormann N, Caires S, Dethof A, Dragosavac M, Fisher M, Fuentes M, Hagemann S, Hólm E, Hoskins BJ, Isaksen L, Janssen PAEM, McNally AP, Mahfouf J-F, Jenne R, Morcrette J-J, Rayner NA, Saunders RW, Simon P, Sterl A, Trenberth KE, Untch A, Vasiljevic D, Viterbo P, Woollen J (2005) The ERA-40 reanalysis. Quart J Roy Meteor Soc 131: 2961-3012

Yanai M, Esbensen S, Chu J-H (1973) Determination of bulk properties of tropical cloud clusters from large-scale heat and moisture budgets. J Atmos Sci 30: 611-627

Yanai M, Chu J-H, Stark TE, Nitta T (1976) Response of deep and shallow tropical maritime cumuli to large-scale processes. J Atmos Sci 33: 976-991

Yanai M, Tomita T (1998) Seasonal and interannual variability of atmospheric heat sources and moisture sinks as determined from NCEP-NCAR reanalyses. J Climate 11: 463-482

Yu R, Zhang M, Cess RD (1999) Analysis of the atmospheric energy budget: a consistency study of available data sets. J Geophys Res 104: 9655-9661